Computational and experimental study of a captive annular eddy

By ENZO O. MACAGNO and TIN-KAN HUNG

Institute of Hydraulic Research, The University of Iowa, Iowa City

Results of calculations and experiments on the flow of a viscous liquid through an axisymmetric conduit expansion are reported. The streamlines and vorticity contours are presented as functions of the Reynolds number of the flow. The dynamic interaction between the main flow and the captive eddy between it and the walls is analysed, and it is concluded that, for laminar flow, the main role of the eddy is that of shaping the flow with a rather small energy exchange.

1. Introduction

In a previous investigation by Hung & Macagno (1966), laminar eddies in the corners of a two-dimensional conduit expansion have been studied using a computational simulation based on discretized forms of the vorticity-transport equation. No quantitative experimental verification was attempted then because, as is well known, it is practically impossible to produce two-dimensional established laminar flows with negligible distortion due to side-wall effects. In the present investigation, laminar flow in an axisymmetric confined flow expansion has been studied both computationally and experimentally.

The laminar flow in an abrupt conduit expansion is characterized by a geometric condition that imposes separation even for very low Reynolds numbers; as a matter of fact, if was found by using the computational model that a zone of separation would exist even for creeping flow. This could not be verified experimentally, but the trend of both computational and experimental flows, as the Reynolds number was made smaller and smaller, appeared to confirm this result. The same result was obtained in the study of the two-dimensional abrupt conduit expansion. One should remember, in this connexion, that in the Jeffery–Hamel flows counterflow always occurs, no matter how small the Reynolds number, if the angle between walls is 180°. In a circular conduit with an expansion, the flow pattern may be looked upon as if composed of a main stream that has generated an annular eddy between itself and the walls and reached a dynamic equilibrium that keeps the annular eddy stationary, captive between the flow that drives it and the walls that tend to slow it down.

The computational simulation was accomplished in two different manners. In the first, which will be called the steady approach, the equations for viscous steady flow were utilized in a finite-difference form for which an iterative numerical scheme was devised to be used in an electronic computer. In the second, or unsteady approach, the local acceleration terms were preserved, and essentially

the same technique of discretization of the differential equations was employed. The procedure followed in the steady approach was to start with a roughly approximate flow pattern for a very low Reynolds number upon which numerical iteration was applied until the finite difference equations were satisfied. Once an acceptable flow pattern was available for a certain Reynolds number, it would be used for calculation with a slightly different Reynolds number, and so on. In the unsteady approach, a flow pattern already known from the steady approach, would be used as the initial one for calculations relative to a quite different
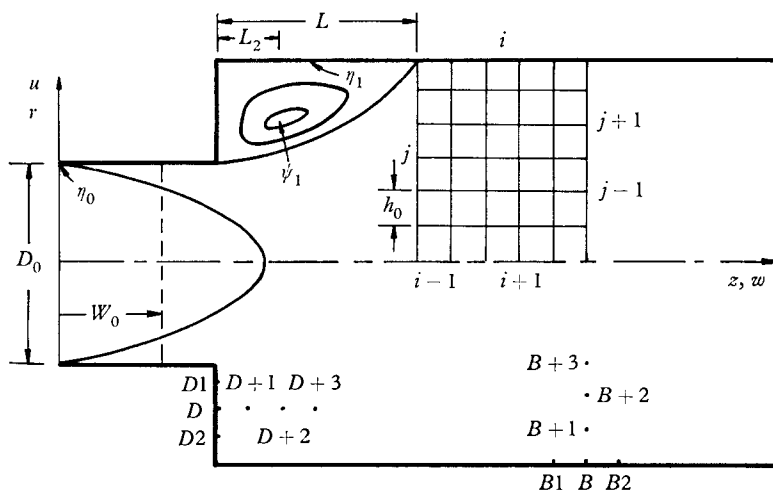

FIGURE 1. Definition sketch.

Reynolds number. It was thought that this process, equivalent to a sudden change in viscosity without varying the rate of flow, would be a smooth one in which the inertia terms would play a stabilizing role. This conjecture proved to be correct and the second approach was found to be more stable, *ceteris paribus*, than the steady approach. In other ways, this has been known to be true, for some time already, to other researchers dealing with finite-difference schemes (Harlow & Fromm 1964; Crocco 1964; Pearson 1965).

The first phase of the investigation consisted in the calculation of the flow and vorticity patterns for different Reynolds numbers. In the second phase, experimental results were obtained and found to agree satisfactorily with those of the computational model. The final phase of the study was then devoted to the calculation of dynamical variables of the flow as well as to the verification of the balances of momentum and impulse, and work and energy, in the computational model. It was the intent of the authors, in this third phase, to provide supplementary information on the dynamic characteristics of an axisymmetric zone of separation in laminar flow, including the quantitative evaluation of the relative importance of the different terms of the momentum and energy equations. Also in view was the interplay between the main flow and the captive annular eddy surrounding it.

The abrupt circular-conduit expansion studied had a diameter ratio of 2 : 1 as

shown in the definition sketch (figure 1). Also shown in the sketch are the parabolic velocity distribution of the Poiseuille flow in the upstream portion of the conduit, and the square mesh used for the finite-difference scheme.

2. Basic equations

For an axisymmetric confined flow of an incompressible fluid, the Navier–Stokes equations in cylindrical co-ordinates are

$$\frac{\partial u}{\partial t} + u\frac{\partial u}{\partial r} + w\frac{\partial u}{\partial z} = -\frac{\partial p}{\partial r} + \frac{1}{R}\left(\frac{\partial^2 u}{\partial r^2} + \frac{1}{r}\frac{\partial u}{\partial r} + \frac{\partial^2 u}{\partial z^2} - \frac{u}{r^2}\right), \tag{1}$$

$$\frac{\partial w}{\partial t} + u\frac{\partial w}{\partial r} + w\frac{\partial w}{\partial z} = -\frac{\partial p}{\partial z} + \frac{1}{R}\left(\frac{\partial^2 w}{\partial r^2} + \frac{1}{r}\frac{\partial w}{\partial r} + \frac{\partial^2 w}{\partial z^2}\right), \tag{2}$$

where u, w, p, t denote the velocity components in the radial and the axial directions, r, z, the pressure, and the time, respectively. The Reynolds number R is based on the upstream diameter D_0 and the mean velocity W_0. All the quantities in (1) and (2) are dimensionless with reference to D_0 and W_0 (figure 1). The equation of continuity is

$$\frac{\partial u}{\partial r} + \frac{\partial w}{\partial z} + \frac{u}{r} = 0. \tag{3}$$

The only non-zero vorticity component is

$$\eta = \frac{\partial u}{\partial z} - \frac{\partial w}{\partial r}. \tag{4}$$

By elimination of the pressure from (1) and (2), the vorticity transport equation

$$\frac{\partial \eta}{\partial t} + u\frac{\partial \eta}{\partial r} + w\frac{\partial \eta}{\partial z} - \frac{u\eta}{r} = \frac{1}{R}\left(\frac{\partial^2 \eta}{\partial r^2} + \frac{1}{r}\frac{\partial \eta}{\partial r} + \frac{\partial^2 \eta}{\partial z^2} - \frac{\eta}{r^2}\right) \tag{5}$$

results. If the Stokes stream function ψ is introduced, (4) and (5) can be expressed as

$$\eta = \frac{1}{r}\left(\frac{\partial^2 \psi}{\partial r^2} - \frac{1}{r}\frac{\partial \psi}{\partial r} + \frac{\partial^2 \psi}{\partial z^2}\right), \tag{6}$$

$$\frac{\partial \eta}{\partial t} + \frac{1}{r}\frac{\partial \psi}{\partial z}\frac{\partial \eta}{\partial r} - \frac{1}{r}\frac{\partial \psi}{\partial r}\frac{\partial \eta}{\partial z} - \frac{\eta}{r^2}\frac{\partial \psi}{\partial z} = \frac{1}{R}\left(\frac{\partial^2 \eta}{\partial r^2} + \frac{1}{r}\frac{\partial \eta}{\partial r} + \frac{\partial^2 \eta}{\partial z^2} - \frac{\eta}{r^2}\right). \tag{7}$$

For the calculation of the pressure, once the functions η and ψ have been determined, the following two integrals of the Navier–Stokes equations can be used:

$$\int_{(r_1, z_1)}^{(r_2, z_1)} \frac{\partial}{\partial r}\left(p + \frac{V^2}{2}\right) dr = \int_{(r_1, z_1)}^{(r_2, z_1)} \left(-w\eta + \frac{1}{R}\frac{\partial \eta}{\partial z}\right) dr, \tag{8}$$

$$\int_{(r_1, z_1)}^{(r_1, z_2)} \frac{\partial}{\partial z}\left(p + \frac{V^2}{2}\right) dz = \int_{(r_1, z_1)}^{(r_1, z_2)} \left(u\eta - \frac{1}{R}\frac{\partial \eta}{\partial r} - \frac{\eta}{Rr}\right) dz, \tag{9}$$

where $V^2 = u^2 + v^2$. The work-energy equation, as was used in this investigation, can be expressed in the following form:

$$\frac{1}{2}\left(u\frac{\partial V^2}{\partial r} + w\frac{\partial V^2}{\partial z}\right) = -\frac{2}{R}\left[\left(\frac{\partial u}{\partial r}\right)^2 + \left(\frac{\partial w}{\partial z}\right)^2 + \left(\frac{u}{r}\right)^2\right] - R\tau^2$$

$$-u\frac{\partial p}{\partial r} - w\frac{\partial p}{\partial z} + \frac{1}{R}\left(\frac{\partial^2 u^2}{\partial r^2} + \frac{\partial^2 w}{\partial z^2} - \frac{2u}{r}\frac{\partial u}{\partial r}\right)$$

$$+ \frac{\partial}{\partial r}(w\tau) + \frac{\partial}{\partial z}(u\tau) + \frac{w\tau}{r}. \tag{10}$$

In this equation, τ represents the dimensionless shearing stress

$$\tau = \frac{1}{R}\left(\frac{\partial u}{\partial z} + \frac{\partial w}{\partial r}\right). \tag{11}$$

The physical meaning of the terms of (10) are, from left to right, convection of kinetic energy, dissipation of energy, work done by pressure, work done by normal viscous stresses, and work done by tangential viscous stresses.

3. Finite-difference equations

For a given system of differential equations, a multiplicity of different sets of difference equations can be formed, and, in this sense, one can consider each of the finite-difference schemes as a distinct simulation of the differential system, or, as a special simulation of the flow represented so accurately by the Navier–Stokes equations. The well-known method of relaxation by Southwell (1940) has been widely applied in engineering and in science. A similar technique, the method of squares, was developed by Thom & Apelt (1961). In the latter method, the function is subject to an iterative process, while in the former one deals with the residues of the finite-difference equations. Thom's techniques are more convenient for calculations with the digital computers, because they save computer storage.

(7) and (6) were written on discrete form, or discretized, by means of common finite-difference formulas and from them the following two expressions were obtained for the vorticity and the stream function:

$$\eta_{i,j}^{k+1} = \left[1 - \frac{R}{2h}(\psi_{i+1,j}^k - \psi_{i-1,j}^k) + \frac{4r_j^2}{h^2}\right]^{-1}\left\{\frac{r_j^2}{h^2}(\eta_{i-1,j}^{k+1} + \eta_{i,j-1}^{k+1} + \eta_{i+1,j}^k + \eta_{i,j+1}^k)\right.$$

$$+ \frac{r_j}{2h}(\eta_{i,j-1}^{k+1} - \eta_{i,j+1}^k) - \frac{Rr_j}{4h^2}[(\psi_{i+1,j}^k - \psi_{i-1,j}^k)(\eta_{i,j-1}^{k+1} - \eta_{i,j+1}^k)$$

$$\left. - (\psi_{i,j-1}^k - \psi_{i,j+1}^k)(\eta_{i+1,j}^k - \eta_{i-1,j}^{k+1})]\right\}, \tag{12}$$

$$\psi_{i,j}^{k+1} = \frac{1}{4}\left[\psi_{i-1,j}^{k+1} + \psi_{i,j-1}^{k+1} + \psi_{i+1,j}^k + \psi_{i,j+1}^k - h^2 r_j \eta_{i,j}^{k+1} - \frac{h}{2r_j}(\psi_{i,j-1}^{k+1} - \psi_{i,j+1}^k)\right], \tag{13}$$

where the subscripts i, j correspond to the z, r co-ordinates, and the superscript k denotes the iterative index; h is the dimensionless mesh size, h_0/D_0.

From experience gained by studying two-dimensional flows, it was already known that a parabolic velocity distribution could be prescribed over a section located at a short distance upstream from the conduit expansion. For the downstream-end section of the region selected for the calculation, the following two extrapolation formulas, derived by Hung (1966), were utilized:

$$\psi_{i,j} = \psi_{i-4,j} - 2\psi_{i-3,j} + 2\psi_{i-1,j}, \tag{14}$$

$$\eta_{i,j} = \eta_{i-4,j} - 2\eta_{i-3,j} + 2\eta_{i-1,j}. \tag{15}$$

Because one works with the stream and the vorticity functions together, not only the non-slip condition

$$\partial\psi/\partial r = 0, \quad \partial\psi/\partial z = 0, \tag{16}$$

must be established for the fixed boundaries, but also expressions for the vorticity are necessary. Through expansion of the stream function ψ in Taylor series, the following expression is obtained:

$$\psi_{B+1} = \psi_B - h\left(\frac{\partial\psi}{\partial r}\right)_B + \frac{h^2}{2!}\left(\frac{\partial^2\psi}{\partial r^2}\right)_B - \frac{h^3}{3!}\left(\frac{\partial^3\psi}{\partial r^3}\right)_B + \frac{h^4}{4!}\left(\frac{\partial^4\psi}{\partial r^4}\right)_B + O(h^5). \tag{17}$$

If one takes into account (6) and (16), one can find the expressions

$$\left.\begin{aligned}
\left(\frac{\partial^2\psi}{\partial r^2}\right)_B &= r_B\eta_B, \quad \left(\frac{\partial^3\psi}{\partial r^3}\right)_B = 2\eta_B + r_B\left(\frac{\partial\eta}{\partial r}\right)_B, \\
\left(\frac{\partial^4\psi}{\partial r^4}\right)_B &= 3\left(\frac{\partial\eta}{\partial r}\right)_B + r_B\left(\frac{\partial^2\eta}{\partial r^2} - \frac{\partial^2\eta}{\partial z^2}\right)_B,
\end{aligned}\right\} \tag{18}$$

for the derivatives of the stream function on the wall parallel to the z-axis. Thus (17) can be written as

$$\psi_{B+1} = \psi_B + \frac{h^2}{2}r_B\eta_B - \frac{h^3}{3!}\left[2\eta_B + r_B\left(\frac{\partial\eta}{\partial r}\right)_B\right]$$
$$+ \frac{h^4}{4!}\left[3\left(\frac{\partial\eta}{\partial r}\right)_B + r_B\left(\frac{\partial^2\eta}{\partial r^2} - \frac{\partial^2\eta}{\partial z^2}\right)_B\right] + O(h^5). \tag{19}$$

If one uses again a Taylor series expansion, the following expression can be obtained:

$$r_B h\left(\frac{\partial\eta}{\partial r}\right)_B = r_B\left[\eta_B - \eta_{B+1} + \frac{h^2}{2!}\left(\frac{\partial^2\eta}{\partial r^2}\right)_B - \frac{h^3}{3!}\left(\frac{\partial^3\eta}{\partial r^3}\right)_B\right] + O(h^4). \tag{20}$$

Substitution of (20) into (19) leads to

$$\psi_{B+1} = \psi_B + \frac{h^3}{3}(r_B - h)\eta_B + \frac{h^2}{6}r_B\eta_{B+1} + \frac{h^4}{8}\left(\frac{\partial\eta}{\partial r}\right)_B - \frac{h^4}{4!}r_B\left(\frac{\partial^2\eta}{\partial r^2} + \frac{\partial^2\eta}{\partial z^2}\right)_B + O(h^5). \tag{21}$$

For steady flow, (7) gives for a point like B (figure 1)

$$\left(\frac{\partial^2\eta}{\partial r^2} + \frac{\partial^2\eta}{\partial z^2}\right)_B = \frac{\eta_B}{r_B^2} - \frac{1}{r_B}\left(\frac{\partial\eta}{\partial r}\right)_B. \tag{22}$$

If use is made of (21) and (22) and of a forward 3-point formula for $(\partial\eta/\partial r)_B$, the following expression for the vorticity at B can be derived:

$$\eta_B = \left(\frac{h^3}{12} + \frac{h^4}{24r_B} - \frac{h^2 r_B}{3}\right)^{-1}\left(\psi_B - \psi_{B+1} + \frac{h^2}{6}r_{B+2}\eta_{B+1} + \frac{h^3}{12}\eta_{B+2}\right) + O(h^3). \tag{23}$$

This formula was also applied to the entrant corner, because separation makes the flow there nearly parallel to the z-axis. For the portion of the conduit wall parallel to the r-axis the boundary vorticity can be expressed by

$$\eta_D = \frac{3}{h^2 r_D}(\psi_{D+1} - \psi_D) - \frac{\eta_{D+1}}{2} + O(h^3). \tag{24}$$

The iteration was continued until the following two conditions were satisfied

$$|\psi_{i,j}^{k+10} - \psi_{i,j}^k|/\psi_0 \leqslant 0.00004, \quad |\eta_{i,j}^{k+10} - \eta_{i,j}^k|/|\eta_0| \leqslant 0.0001, \tag{25}$$

in which ψ_0 represents the discharge divided by 2π and η_0 the value of the wall vorticity at the inlet.

The time-dependent equation (7) used in the unsteady approach can be discretized by means of central-difference formulas, and from it the following expression of the vorticity can be obtained:

$$\eta_{i,j}^{n+1} = \left(\frac{Rr_j^2}{2\delta t} + \frac{4r_j^2}{h^2} + 1\right)^{-1} \left\{\frac{Rr_j^2}{2\delta t}\eta_{i,j}^{n-1} - \frac{Rr_j}{4h^2}\left[(\psi_{i+1,j}^n - \psi_{i-1,j}^n)(\eta_{i,j-1}^n - \eta_{i,j+1}^n)\right.\right.$$

$$\left. - (\psi_{i,j-1}^n - \psi_{i,j+1}^n)(\eta_{i+1,j}^n - \eta_{i-1,j}^n) - \frac{R}{2h}(\psi_{i+1,j}^n - \psi_{i-1,j}^n)\eta_{i,j}^n\right]$$

$$\left. + \frac{r_j^2}{h^2}(\eta_{i-1,j}^n + \eta_{i,j-1}^n + \eta_{i+1,j}^n + \eta_{i,j-1}^n) + \frac{r_j}{2h}(\eta_{i,j-1}^n - \eta_{i,j+1}^n)\right\}. \tag{26}$$

After one computes the vorticity η^{n+1}, at $t = (n+1)\delta t$, from the values of ψ and η at two preceding times, the corresponding stream function can be calculated, by iterative operations, from

$$\psi_{i,j}^{n+1} = \tfrac{1}{4}[\psi_{i-1,j}^{n+1} + \psi_{i,j-1}^{n+1} + \psi_{i+1,j}^{n+1} + \psi_{i,j+1}^{n+1} + \tfrac{1}{2}hr_j^{-1}(\psi_{i,j-1}^{n+1} - \psi_{i,j+1}^{n+1}) - h^2 r_j \eta_{i,j}^{n+1}]. \tag{27}$$

The next step is to calculate the boundary vorticity for $t = (n+1)\delta t$ according to the procedure indicated in the following. It is, at first, considered that the term

$$\frac{h^4}{4!}r_B\left(\frac{\partial^2 \eta}{\partial r^2} + \frac{\partial^2 \eta}{\partial z^2}\right)_B$$

in (21) is negligible, and the vorticity on the wall parallel to the z-axis is obtained from

$$\eta_B = \left(\frac{h^2}{3}r_{B+1} + \frac{3h^3}{16}\right)^{-1}\left[\psi_{B+1} - \psi_B - \left(\frac{h^2}{6}r_B - \frac{h^3}{4}\right)\eta_{B+1} - \frac{h^3}{16}\eta_{B+2}\right]. \tag{28}$$

Similarly, for the wall parallel to the r-axis, one obtains

$$\eta_D = \left(\frac{h^2}{3}r_D + \frac{h^4}{24r_D} + \frac{h^3}{16}\right)^{-1}\left[\psi_{D+1} - \psi_D - \left(\frac{h^2}{6}r_D - \frac{h^3}{12}\right)\eta_{D+1} - \frac{h^3}{48}\eta_{D+2}\right]. \tag{29}$$

Once all the boundary values have been calculated, a better set of values can be evaluated, through iteration, from

$$\eta_B = \left(\frac{h^2}{3}r_{B+1} + \frac{3h^3}{16}\right)^{-1}\left[\psi_{B+1} - \psi_B - \left(\frac{h^2}{6}r_B - \frac{h^3}{4}\right)\eta_{B+1}\right.$$
$$\left. - \frac{h^3}{16}\eta_{B+2} + \frac{h^2}{24}r_B(\eta_{B1} + \eta_{B2} - 5\eta_{B+1} + 4\eta_{B+2} - \eta_{B+3})\right], \quad (30)$$

$$\eta_D = \left(\frac{h^2}{3}r_D + \frac{h^4}{24r_D} + \frac{h^3}{16}\right)^{-1}\left[\psi_{D+1} - \psi_D - \left(\frac{h^2}{6}r_D - \frac{h^3}{12}\right)\eta_{D+1}\right.$$
$$\left. - \frac{h^3}{48}\eta_{D+2} + \frac{h^2}{24}r_D(\eta_{D1} + \eta_{D2} - 5\eta_{D+1} + 4\eta_{D+2} - \eta_{D+3})\right]. \quad (31)$$

The first of these two expressions for the vorticity at a point B was obtained by replacing $\partial^2\eta/\partial r^2$ and $\partial^2\eta/\partial z^2$ in (21) by their finite-difference expressions. The second was derived in a similar fashion. The vorticity on the concave corner was set equal to zero, and at the adjacent points (23) and (24) were used; only on these three boundary points was the iteration procedure not applied. This kind of boundary treatment proved to be satisfactory in a related study of flow suddenly accelerated from rest in a two-dimensional conduit expansion.

4. Previous verification of the computational model

As a means of verifying the accuracy of the difference scheme set up for this investigation and of testing its computational stability, the system of difference equations for the flow and for the boundary conditions was applied to a dis-
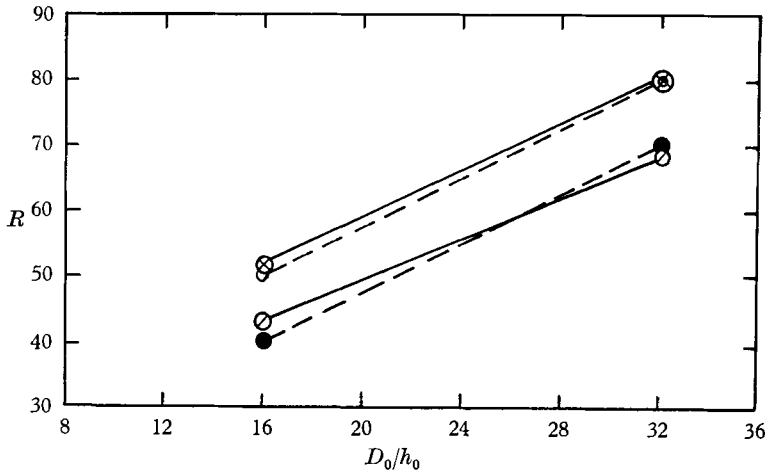

FIGURE 2. Stability of numerical solutions for steady axisymmetric flow. Flow with separation: $\bigcirc$, divergence; $\bullet$, convergence. Disturbed uniform flow: $\otimes$, four-way iteration; $\oslash$, one-way iteration.

turbed uniform flow obtained by altering the known values of the vorticity in a Poiseuille uniform flow in a certain regular pattern; i.e. by increasing and decreasing the vorticity in a given proportion at alternate points. This disturbed distribution of the vorticity was adopted as a condition initially existing in the

Enzo O. Macagno and Tin-Kan Hung

fluid, and the calculations were run in the electronic computer according to the
general programme for the flow in the conduit expansion. Were the system com-
putationally unstable, it was reasoned, the disturbed flow would fail to come
back to the original uniform flow; were the system stable, but still convergent to
a different solution, this would also be discovered. Figure 2 shows results of these
tests and the slight influence of sweeping the field in different ways during the
iteration. Also in the same figure are shown results obtained for the flow through
the conduit expansion. They confirm the expectancy that the disturbed uniform

D_0/h_0	R	e	k	r/D_0 $\frac{1}{2}$	$\frac{3}{8}$	$\frac{1}{4}$	$\frac{1}{8}$	0
						ψ		
16	20	0·1	20	0	0·023799	0·070097	0·109718	0·125000
16	20	0·1	60	0	0·023780	0·070098	0·109718	0·125000
16	20	0·1	100	0	0·023780	0·070098	0·109718	0·125000
32	79	0·5	32	0	0·024024	0·070401	0·109801	0·125000
32	79	0·5	128	0	0·023897	0·070263	0·109831	0·125000
Exact values of ψ				0	0·023925	0·070312	0·109863	0·125000
						η		
16	20	0·1	20	7·937101	5·958431	3·979629	1·993172	0
16	20	0·1	60	7·937226	5·958553	3·979673	1·993182	0
16	20	0·1	100	7·937226	5·958553	3·979673	1·993182	0
32	79	0·5	32	8·049248	5·999148	3·994859	1·925871	0
32	79	0·5	128	7·982371	5·991121	3·985256	1·999934	0
Exact values of η				8·000000	6·000000	4·000000	2·000000	0

Verification of the computational scheme by calculating Poiseuille flow in a circular tube
starting from an initial distribution of vorticity disturbed by alternately applied factors
$(1 \pm e)$; k is the index of iteration.

TABLE 1. Numerical solutions of Poiseuille flow in a circular pipe.

flow would predict with reasonable accuracy the behaviour of the computational
model for non-uniform flow, at least for cases in which the non-uniformity is not
extreme to the point of disrupting the flow much more than the purposely
introduced disturbances of the flow in the uniform conduit. To convey a numerical
impression of the indications obtained from the technique of disturbing the
uniform flow, table 1, which is self-explanatory, is presented.

5. Results of the computations

A series of flow patterns in the conduit expansion is presented in figures 3 and 4
for several Reynolds numbers from a vanishingly small value up to 70. The values
of the dimensionless stream and vorticity functions are given in two of the dia-
grams; for the other four, the same values apply unless otherwise indicated. As
in the case of two-dimensional flow, a small corner eddy was found for creeping
motion; about the same eddy size but a little higher intensity was also found for
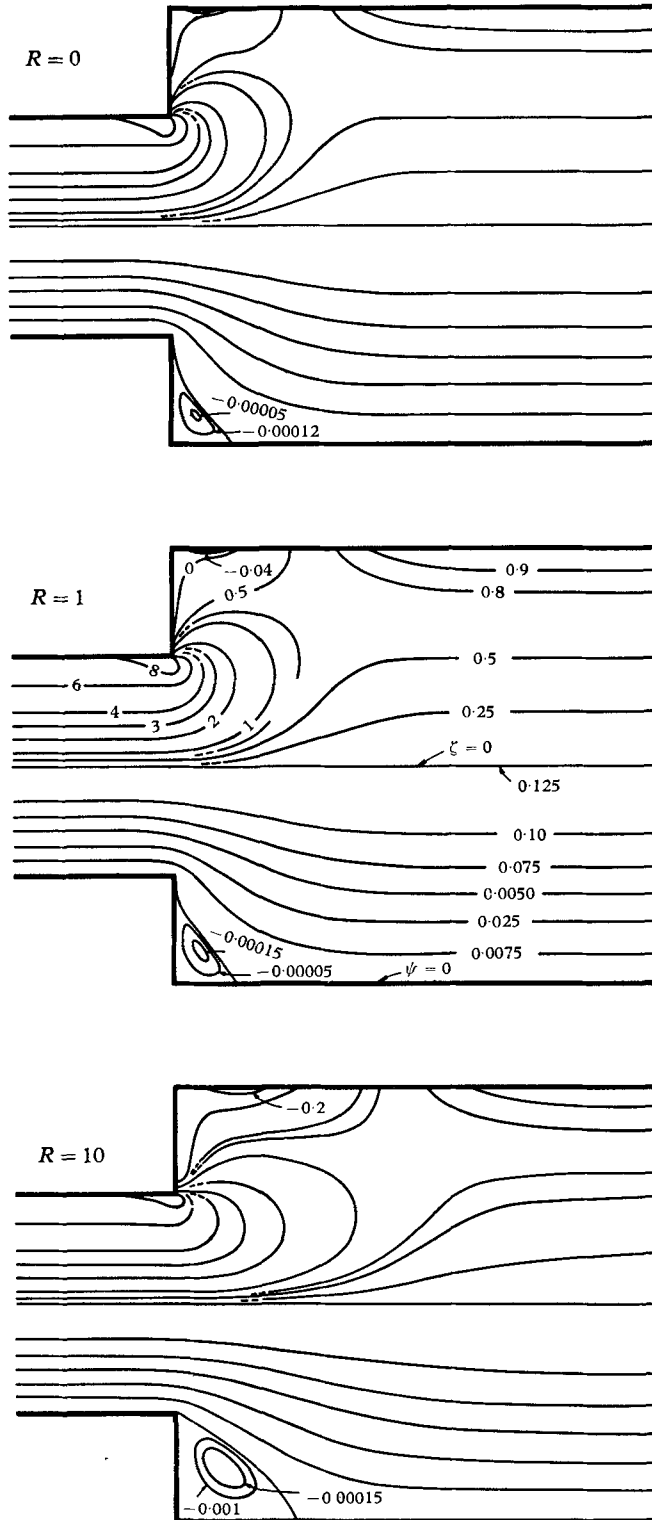$R = 1$. For $R = 0$, the equation for the stream function becomes $E^4\psi = 0$ (see

FIGURE 3. Vorticity contours and streamlines obtained by steady approach.
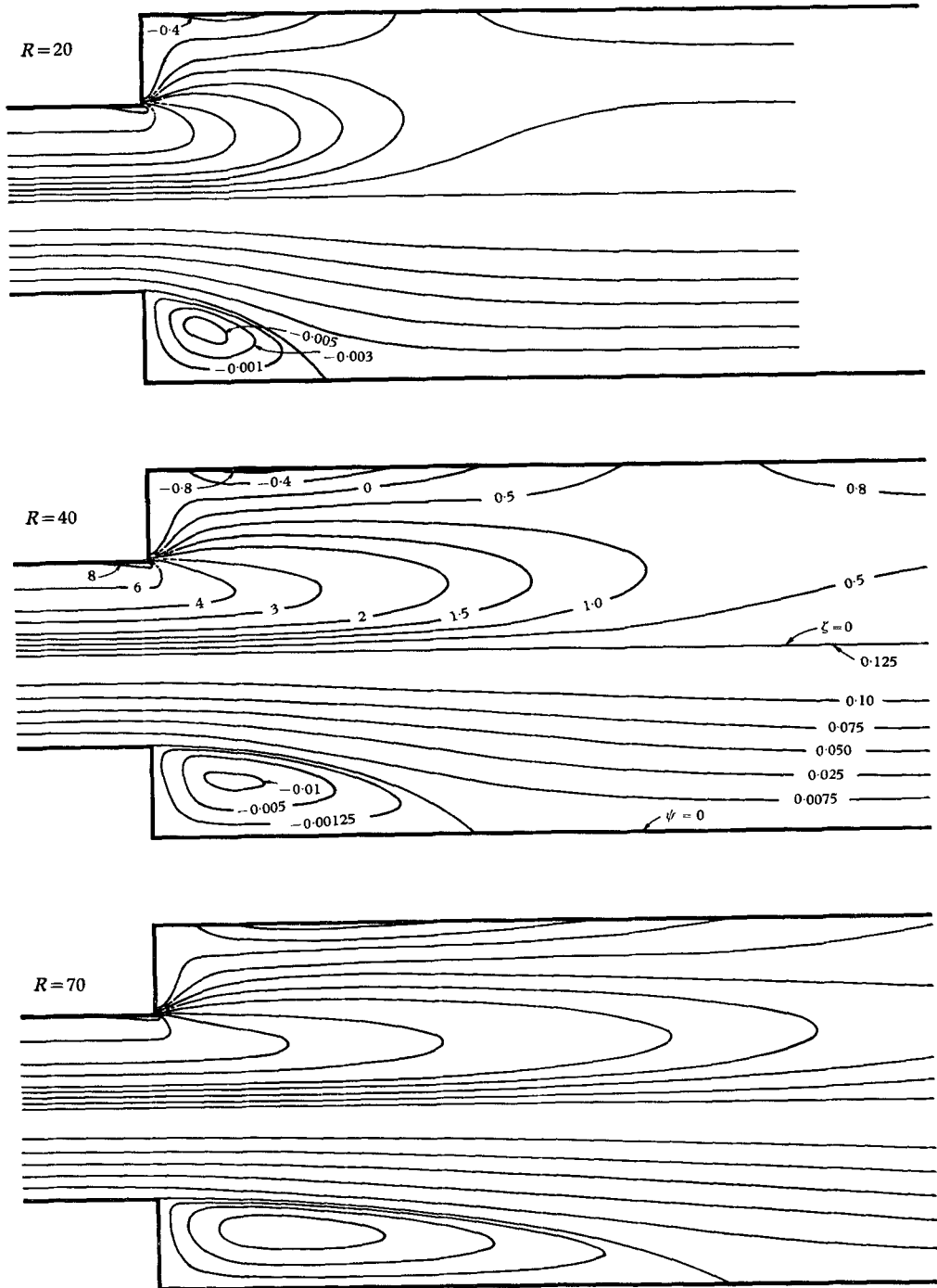
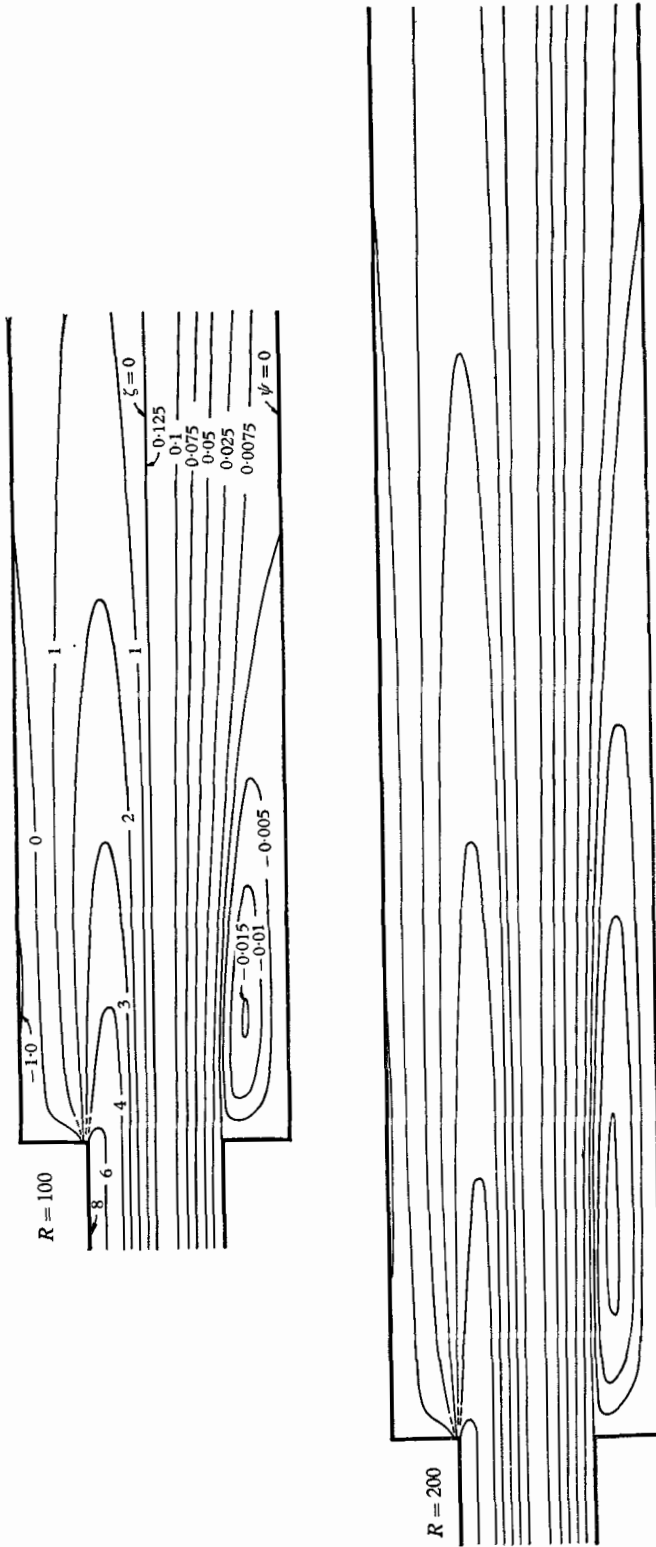FIGURE 4. Vorticity contours and streamlines obtained by steady approach.

FIGURE 5. Vorticity contours and streamlines obtained by unsteady approach.

Milne-Thomson 1950); the authors are not aware of any theoretical result that
would indicate that in such a case the function ψ could not take an extreme value
in the interior of the flow, and they therefore tend to accept the results of the
calculations as an indication of the possibility of eddies occurring in creeping
flow whenever the geometry favours their existence. The vorticity lines shown
in figures 3 and 4 are stretched in the direction of the flow as the Reynolds
number becomes larger; it is obvious that the peak of the vorticity cannot
coincide with the separation line, because otherwise a contradiction would result
at the reattachment point, where the vorticity must be zero. In fact, the vorticity
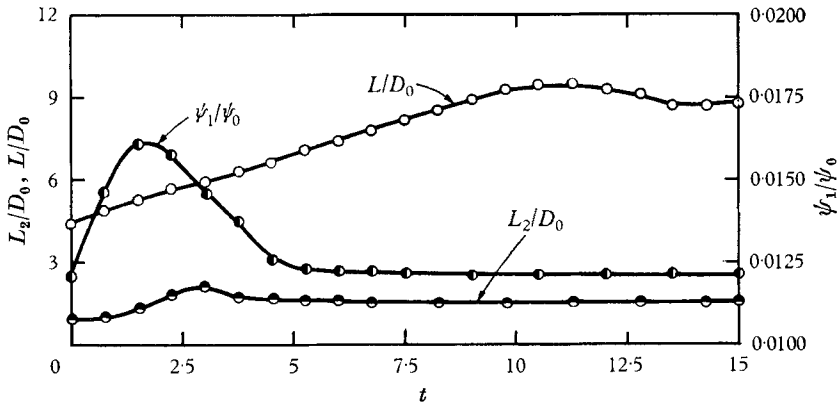
FIGURE 6. Time variations of the relative eddy length L/D_0, the relative eddy intensity ψ_1/ψ_0,
and the relative location of eddy centre L_2/D_0, for a variation of the Reynolds number from
100 to 200.

peak first moves into the main flow when separation occurs, and then moves
back to the wall well downstream from the stream-reattachment point.

The stream and vorticity lines shown in figure 5 for $R = 100$ and $R = 200$ were
obtained using the unsteady approach; for the same mesh size, the steady
approach would have been unstable. No effort was made in this investigation to
analyse or test the computational stability of the unsteady approach, but the
criteria for the two-dimensional flows (Hung & Macagno 1966) were followed and
the results were satisfactory. The unsteady approach was verified by determining
the flow pattern for $R = 40$ for which it was already known through the steady
approach. The variations of eddy length, eddy intensity and the location of its
centre during the process of going from $R = 100$ to $R = 200$ are shown in figure 6.

6. Experimental investigation

The experimental apparatus used for the experiments resulted from a tempor-
ary adaptation of an oil-circulating unit normally employed for laboratory
instruction on laminar and turbulent flow (figure 7, upper part). The unit consists
of an oil reservoir from which a pump impels the oil through a bronze pipe, at the
outlet of which it is received in a weighing device; after being weighed, the oil is
returned to the reservoir. Part of the pipe was replaced by a conduit of the same

diameter with an abrupt expansion that had been machined coaxially in a prism of transparent material (figure 7, lower part).

The flow at the expansion was observed by means of fine tracers suspended in the oil, because it was considered that this would disturb the flow the least and
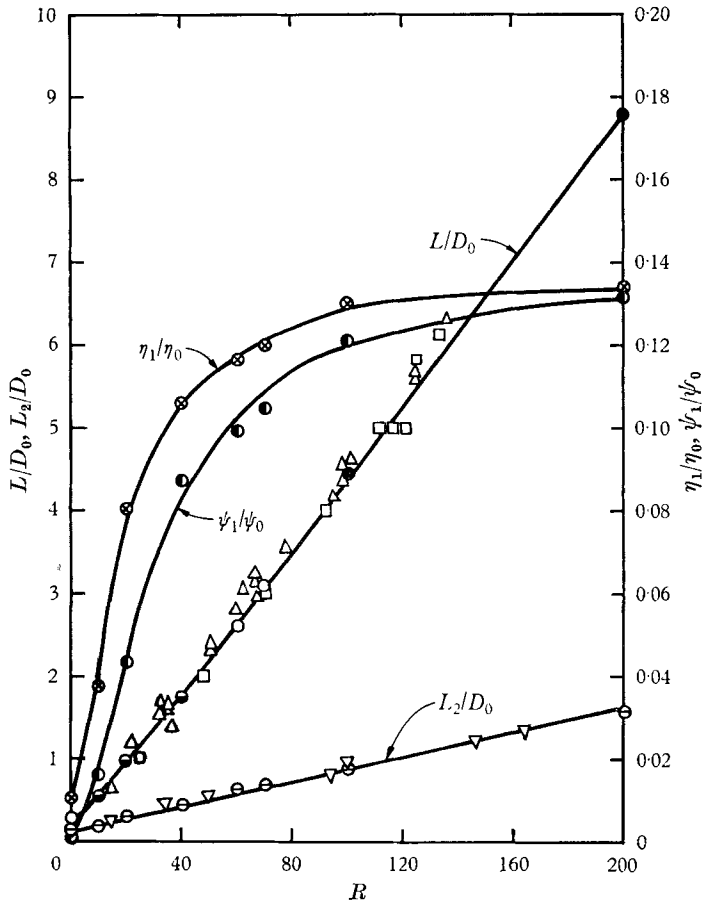

FIGURE 10. Characteristics of the annular eddy as functions of the Reynolds number; L/D_0, relative length; L_2/D_0, relative location of the eddy centre; ψ_1/ψ_0, relative eddy intensity; η_1/η_0, relative maximum vorticity in the backflow region. Steady approach: $\ominus$, $h = \frac{1}{16}$; O, $h = \frac{1}{32}$. Unsteady approach: $\bullet$, $h = \frac{1}{16}$. Experiment: $\nabla\triangle$, photograph; $\square$, dye.

provide a visualization of the streamlines that could be recorded photographic-ally. The photographic technique employed was very similar to the one developed by Macagno at the Iowa Institute of Hydraulic Research eight years ago (see Macagno & Rouse 1961). The photographic information was supplemented with direct visual observation of dyed oil coming into the flow through a series of small orifices bored through the walls of the conduit (figure 7). The dyed filaments behaved usually in a deceptive way, but they were very useful in detecting the point (or line) of reattachment of the separation streamline; to do this, the rate of flow was so adjusted that the separation streamline would meet the wall at the middle orifice of a group of three through which the dyed fluid was being injected.

The tracer used was aluminium powder, a small quantity of which was added to the oil and distributed uniformly by running the unit for several minutes at maximum rate of flow under turbulent conditions. When using the photographic technique mentioned above, an axial plane was illuminated and time exposures were taken in such a manner that the flow pattern of both the eddy and the main flow could be recorded. In figure 8, the experimentally obtained flow patterns for Reynolds numbers of 36 and 4500 are shown; for the latter case, two flow patterns are presented; one corresponds to laminar flow and the other to turbulent flow. The laminar flow for $R = 4500$ was not really axisymmetric; a cellular secondary flow could be observed through the transparent walls, which resulted in a slow helicoidal motion of the tracer particles. The turbulent condition for $R = 4500$ was induced by disturbing the flow purposely at the inlet of the pipe.
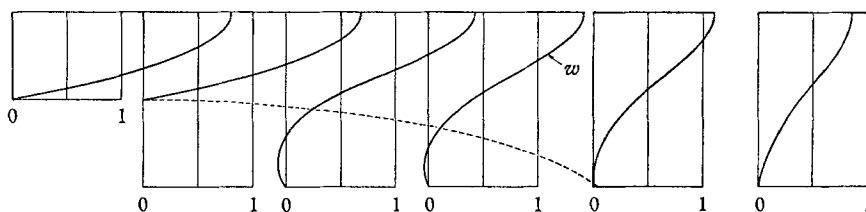
FIGURE 11. Velocity profiles for the component w.

Comparison between experiment and calculation is shown in figure 9 for three Reynolds numbers: 61, 101, and 198 for the actual flow, and the slightly different 60, 100, and 200 for the computationally simulated flow. The relations between the kinematic characteristics of stationary eddies and the Reynolds number of the flow are shown in figure 10 between 40 and 200, the line for the relative length of the eddy L/D_0 is very nearly straight; between 0 and 40 it curves slightly upwards, and it takes a value of $L/D_0 = 0.27$ at $R = 0$. The experimental values, determined from photographic records and from direct observations of the direction in which dyed fluid would move, fall quite close to the calculated values. The relative location of the centre of the eddy L_2/D_0 is also represented in figure 10; and shows a good agreement between experiment and calculation; a straight line fits all points very well. Two other kinematic characteristics appear in figure 10; they are the relative eddy intensity, and the ratio of the absolute value of the maximum wall vorticity in the backflow region to the boundary vorticity on the wall in the upstream uniform flow. The two curves show a similar trend and appear to have asymptotic limits; this should be expected because, although the eddy length may tend to grow indefinitely, its relative strength should not grow once it becomes long enough to have a central portion over which the flow conditions of flow and counterflow become very nearly uniform.

7. Dynamic characteristics of the flow

The flow with $R = 60$ was chosen for calculations of the Bernoulli sum, the pressure, the viscous stresses, and the different terms of the momentum and energy equations. For this Reynolds number, the relative length of the eddy is not
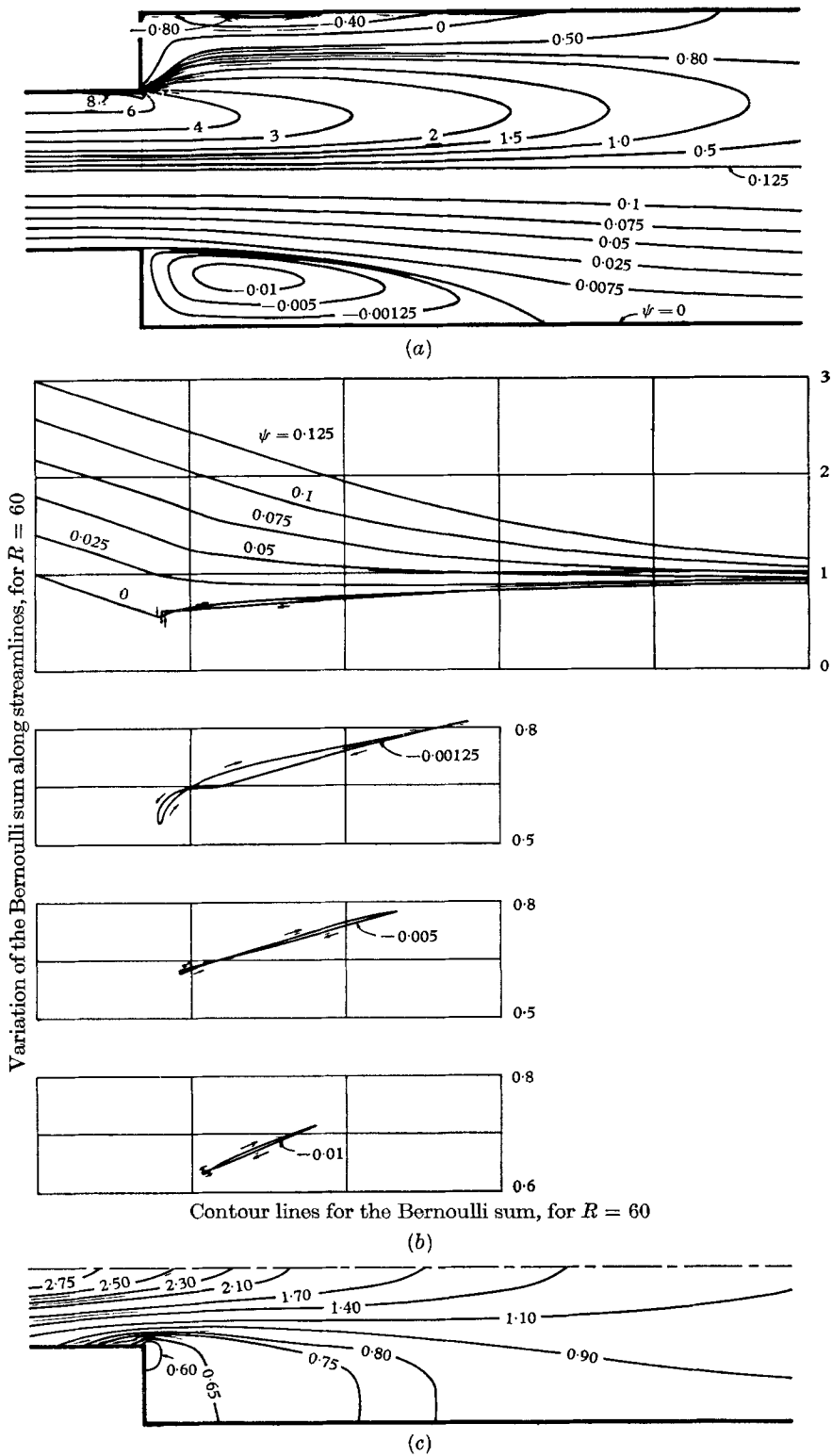
(a)

Contour lines for the Bernoulli sum, for $R = 60$

(b)

(c)

FIGURE 12. (a) Vorticity contours and streamlines, for $R = 60$. (b) Variation of the Bernoulli sum along streamlines, for $R = 60$. (c) Contour lines for the Bernoulli sum, for $R = 60$.

too great and the intensity is high enough to constitute an interesting case with effective influence of the flow curvature. For these calculations, a dimensionless mesh size of $\frac{1}{16}$ was used, while the basic data relative to ψ and η were obtained with a mesh size of $\frac{1}{32}$. Velocity diagrams are given for several cross-sections in figure 11; it can be noticed that the relative intensity of the flow in the eddy is very small. In figure 12 a, the streamlines and the vorticity contours for $R = 60$ are given, while in figure 12 b the variation of the Bernoulli sum B along several streamlines has been represented; contour lines for B are given in figure 12 c. Whether the Bernoulli sum increases or decreases in the direction of the flow depends on the relative values and signs of the two terms in the right-hand side of the following equation:

$$\int_{S_1}^{S_2} dB = \int_{S_1}^{S_2} \frac{1}{V} \left[\frac{\partial}{\partial r} \left(\frac{2u}{R} \frac{\partial u}{\partial r} + w\tau \right) + \frac{\partial}{\partial z} \left(\frac{2w}{R} \frac{\partial w}{\partial z} + u\tau \right) + \frac{2u}{Rr} \frac{\partial u}{\partial r} + \frac{w\tau}{r} \right] ds$$
$$- \int_{S_1}^{S_2} \frac{1}{V} \left[\frac{2}{R} \left(\frac{\partial u}{\partial r} \right)^2 + \frac{2}{R} \left(\frac{\partial w}{\partial z} \right)^2 + \frac{2u^2}{Rr^2} + R\tau^2 \right] ds, \quad (32)$$

where S_1 and S_2 represent two points on a streamline. The first integral on the right side represents the effect of transfer of energy by viscous stresses, while the second expresses that of the dissipation of energy.

The pressure distribution (figure 13 a) shows the expected adverse pressure gradient, which goes well beyond the point of reattachment; at the downstream end, the pressure contours do not seem very satisfactory, but one should bear in mind that there the flow is still far from uniform. The three normal viscous stresses are given in contour representation in figures 13 b–d, and the contours for shearing stresses are given in figure 13 e. The numerical sum of the normal stresses at all points of the field was verified, because it should be zero according to the equation of continuity; it was found to be less than 10^{-5} everywhere, except in a small region near the point of separation where relatively large errors were obtained. The expressions used to evaluate shearing stresses were the following:

$$\tau = R^{-1}(\eta - 2\,\partial w/\partial r), \quad \tau = R^{-1}(2\,\partial u/\partial z - \eta). \quad (33)$$

The first of these two expressions was applied at the inlet and outlet sections and on the normal wall; for the rest of the field, the second formula was used.

The momentum integral along the conduit was computed to verify the balance of momentum flux and forces in the longitudinal direction. As can be seen from figure 14, eight subregions were used for evaluating the surface integral in the impulse-momentum equation

$$\int_S w^2 \frac{\partial z}{\partial n} dS = - \int_S p \frac{\partial z}{\partial n} dS + \int_S \tau \frac{\partial r}{\partial n} dS + \frac{2}{R} \int_S \frac{\partial w}{\partial z} \frac{\partial z}{\partial n} dS, \quad (34)$$

where S denotes the total surface of the wall and cross-sections. The last term on the right side is zero because of the equation of continuity; therefore, the loss of momentum flux is due to the differential pressure force on the cross-sectional areas and the shear force on the boundary. The jump in the pressure-force curve

represents the drag on the normal wall as evaluated from direct integration of the pressure. The residue line shows relatively small values.

The pointwise verification of the Navier–Stokes equations was carried out with the two expressions

$$u \, \partial u/\partial r + w \, \partial u/\partial z + \partial p/\partial r - R^{-1} \, \partial \eta/\partial z = 0, \tag{35}$$

$$u \, \partial w/\partial r + w \, \partial w/\partial z + \partial p/\partial z + R^{-1} \, (\partial \eta/\partial r + u/r) = 0. \tag{36}$$
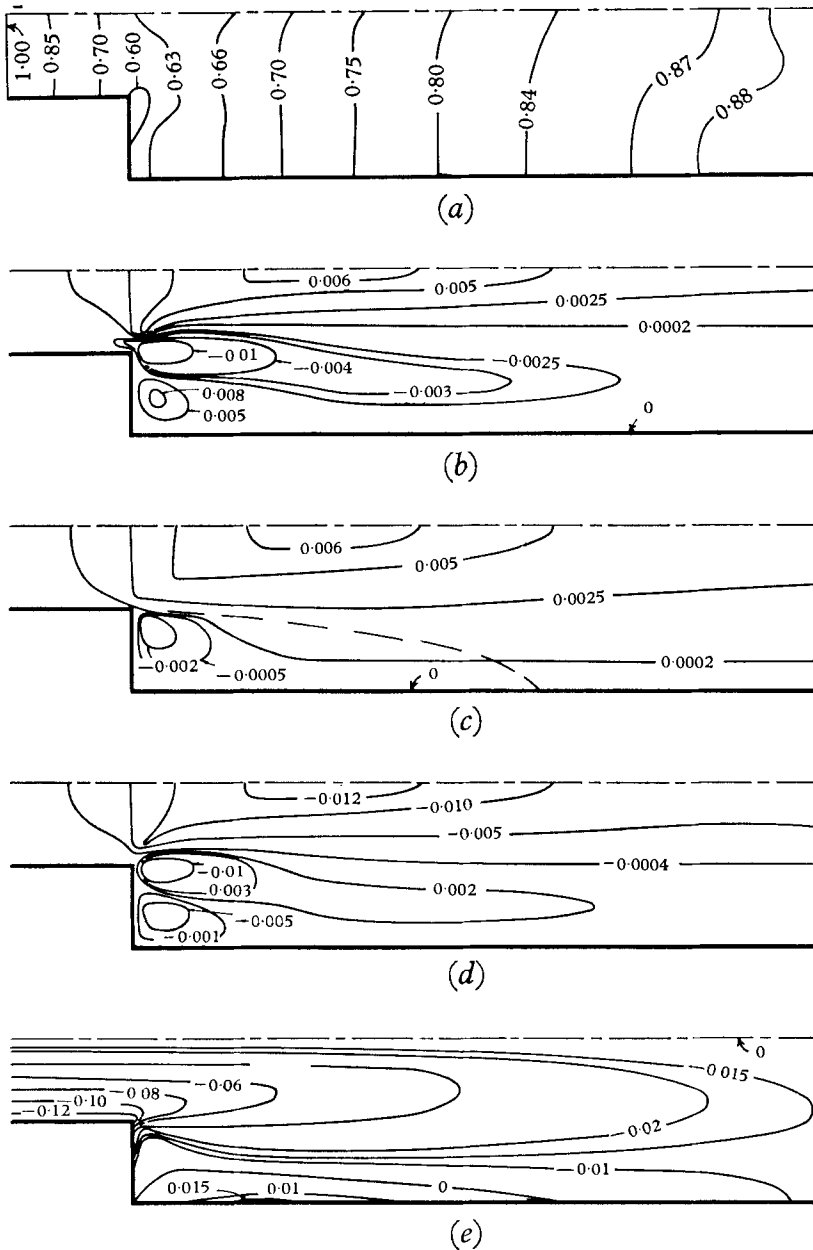
FIGURE 13. From *a* to *e*: contours for the pressure *p*, the three normal viscous stresses in the directions *r*, *θ*, *z*, and the tangential viscous stress *τ*, for *R* = 60.

The residues for these equations are shown in figure 15, as r_r and r_z, respectively. The numerical model employed in this research was tested by applying it to a uniform Poiseuille axisymmetric flow and it showed larger relative errors than
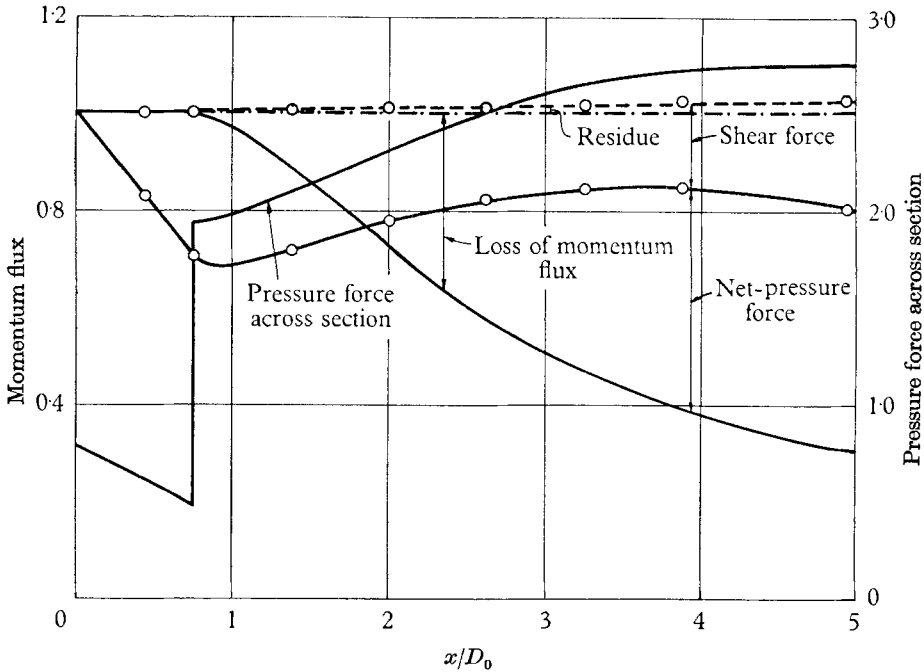
FIGURE 14. Balance of momentum flux and forces along the conduit, for $R = 60$.
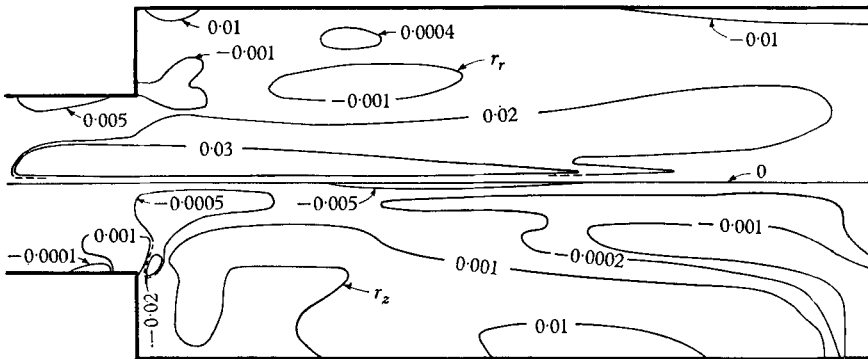
FIGURE 15. Residues r_r and r_z, for $R = 60$.

the similar model for plane Poiseuille flow; therefore, it is not surprising that the residues shown in figure 15 are also larger than the corresponding values found in a previous investigation of two-dimensional conduit expansions (Hung & Macagno 1966).

Figure 16, a to e, shows in contour forms the variation of the five terms of the

(a)

(b)

(c)

(d)

(e)

(f)
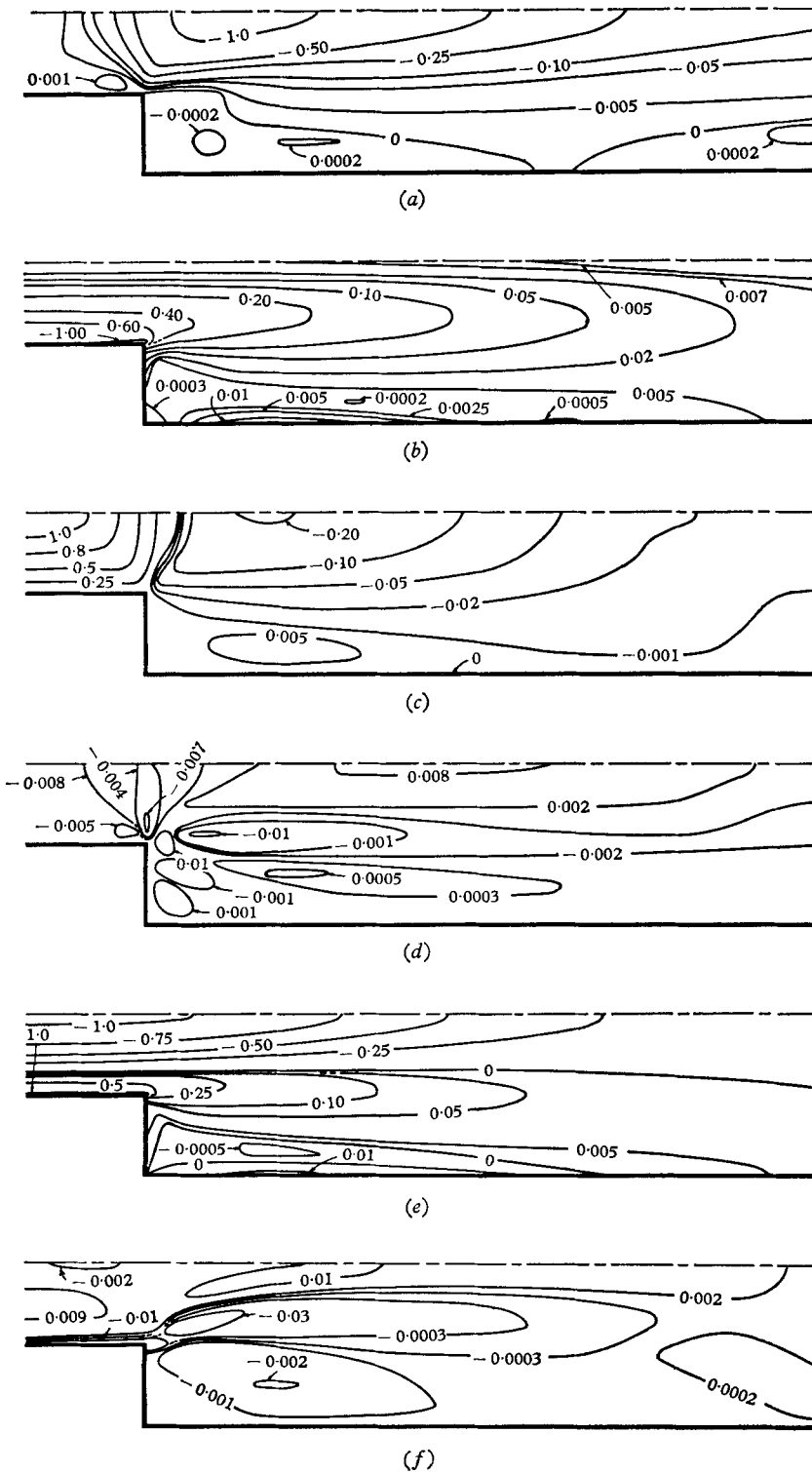
FIGURE 16. From *a* to *e*: convection of kinetic energy, dissipation of energy, and work done by pressure, normal stresses and tangential stresses. The diagram *f* represents the residues of the work-energy equation. Calculations for $R = 60$.

work-energy equation, and in diagram f, the corresponding residues. The rate of dissipation of energy was evaluated from the following expressions:

$$\frac{4}{R}\left(\frac{u^2}{r^2} - \frac{\partial u}{\partial r}\frac{\partial w}{\partial z}\right) + R\tau^2, \quad \frac{2}{R}\left(\frac{\partial^2 u^2}{\partial r^2} - 2\frac{\partial u}{\partial r}\frac{\partial w}{\partial z}\right) + R\tau^2.$$

The second was used along the axis of symmetry, while the first was applied on the rest of the field. Along the z-axis, or conduit axis, the rates at which work is done by normal and tangential viscous stresses were calculated, respectively, with the expressions:

$$R^{-1}(2\,\partial^2 u^2/\partial r^2 + \partial^2 w^2/\partial z^2) \quad \text{and} \quad 2w(\partial\tau/\partial r).$$
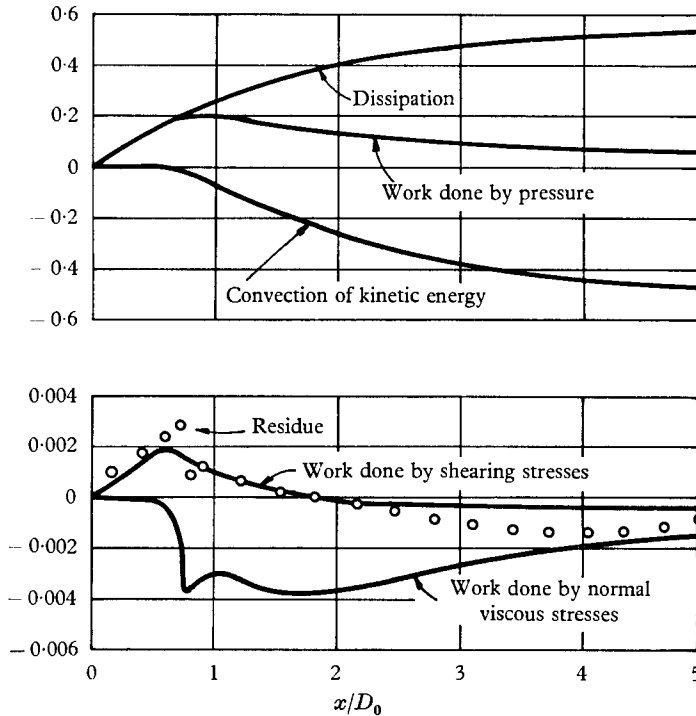
FIGURE 17. Balance and work and energy along the conduit, for $R = 0.6$

Within the eddy, the fluid moves very slowly and most of the values of terms of the work-energy equation are very small. For instance, the convection and the dissipation of energy there are very small, and the obvious conclusion is that the role of these eddies is more one of shaping the main flow than one of exchange and dissipation of energy. This should also be true of rather long eddies, because the ratio of the intensity of the eddy flow and the intensity of the main flow seems to tend to a constant value (figure 10). The integrated form of the work-energy equation has been used to calculate the values represented in the upper diagram of figure 17, for the dissipation of energy, the work done by the pressure, and the convection of kinetic energy, which are very approximately in balance. The other two terms, the work done by tangential and normal viscous stresses, are

very small and had to be represented in the lower diagram at a different scale. In this lower diagram, the residues also appear, and have the same order of magnitude as the terms of the work-energy equation plotted there. It can, therefore, be concluded that the integrated form of the work-energy equation can be reduced to a simplified form in which the work of the viscous stresses may be neglected.

8. Concluding remarks

The annular, laminar, captive eddy in a conduit expansion has been studied in detail, by means of a computational simulation, for an expansion ratio of 2 : 1 and for Reynolds numbers up to 200. Experimentally, the same flow has also been observed, and good agreement exists between the calculations and the experiments.

The computational model has been operated in two different manners, both with explicit forms of the finite-difference scheme utilized, but preserving in one the local acceleration terms while eliminating them from the other. For high Reynolds numbers, the unsteady approach exhibited a higher computational stability, other things being equal. When both models were stable, the numerical results were practically coincident.

The study of the dynamic characteristics of the annular eddy and of the sustaining main flow revealed that the role of the first is principally that of helping to shape the second in a streamlined fashion and without much exchange of energy. The results of the calculations of dynamic characteristics give an overall picture with internal consistency, exhibiting small residues except at a few points in which a finer mesh than the ones used should be employed. The interested forms of the momentum-impulse and work-energy equations present a very satisfactory first-order-of-magnitude balance; it can also be concluded that the work-energy relationship in its integrated form is reducible to only three of its five terms, because the two terms representing the rate at which work is done by viscous stresses are negligibly small.

REFERENCES

CROCCO, L. 1964 Solving numerically the Navier–Stokes equations. *General Electric Co. Doc.* no. 63SD891.

HARLOW, F. H. & FROMM, J. E. 1964 Dynamics and heat transfer in the von Kármán wake of a rectangular cylinder. *Phys. Fluids*, **7**, 1147.

HUNG, T. K. 1966 Laminary flow in conduit expansions. Ph.D. Dissertation. The University of Iowa.

HUNG, T. K. & MACAGNO, E. O. 1966 Laminar eddies in a two-dimensional conduit expansion. *La Houille Blanche* (to be issued).

MACAGNO, E. O. & ROUSE, H. 1961 Interfacial mixing in stratified flow. *J. Engng Mech. EMS*, paper 2964.

MILNE-THOMSON, L. M. 1950 *Theoretical Hydrodynamics*. New York: MacMillan.

PEARSON, C. E. 1965 A computational method for viscous flow problems. *J. Fluid Mech.* **21**, 611.

SOUTHWELL, R. V. 1940 *Relaxation Methods in Engineering Science*. Oxford University Press.

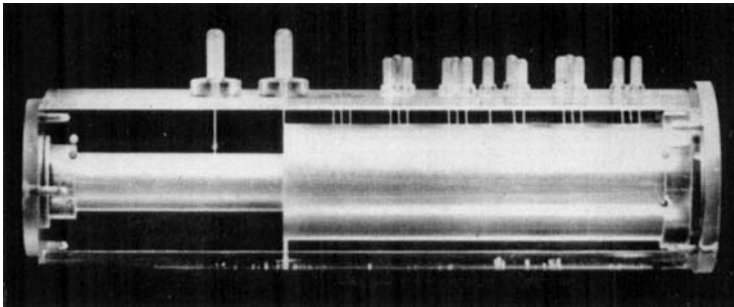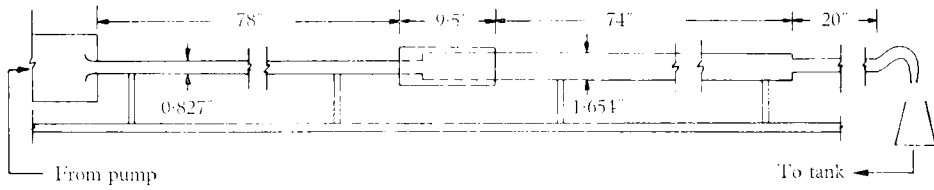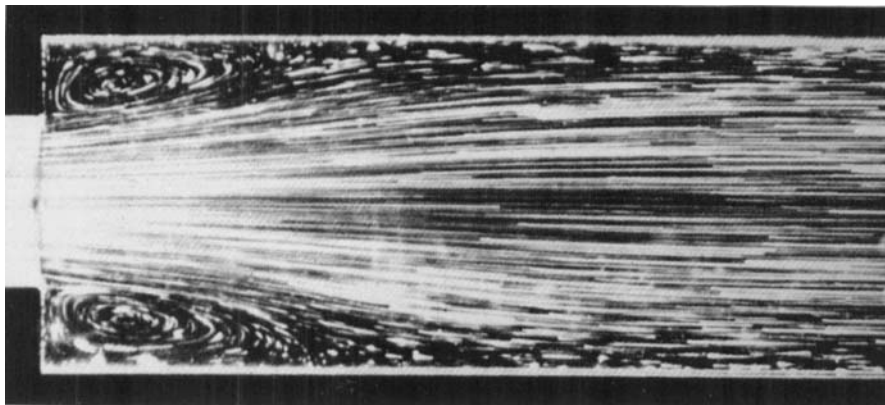THOM, A. & APELT, C. J. 1961 *Field Computations in Engineering and Physics*. London: D. Van Nostrand.
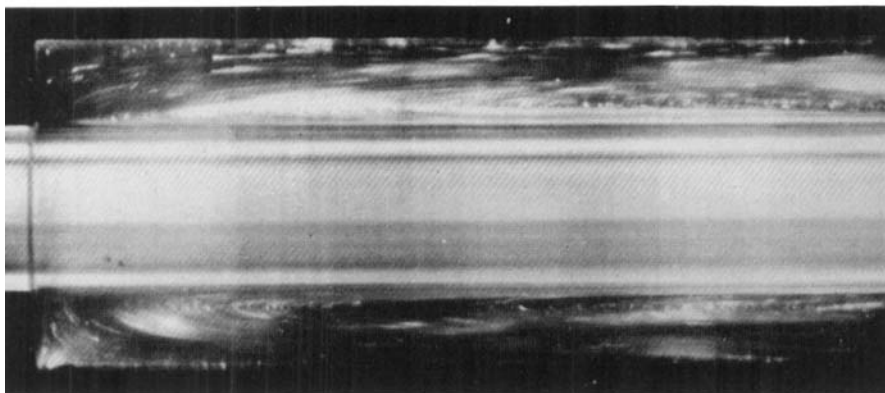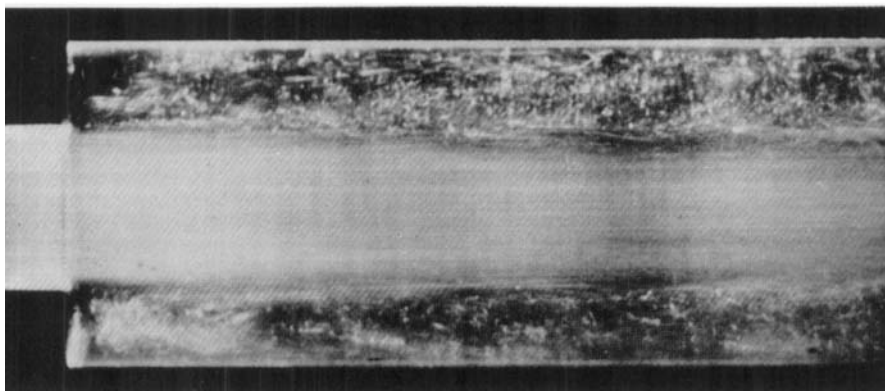
FIGURE 7. Experimental apparatus.

$R = 36$

$R = 4500$

$R = 4500$ (turbulent)

FIGURE 8. Photographic record of the flow in an axisymmetric conduit expansion.
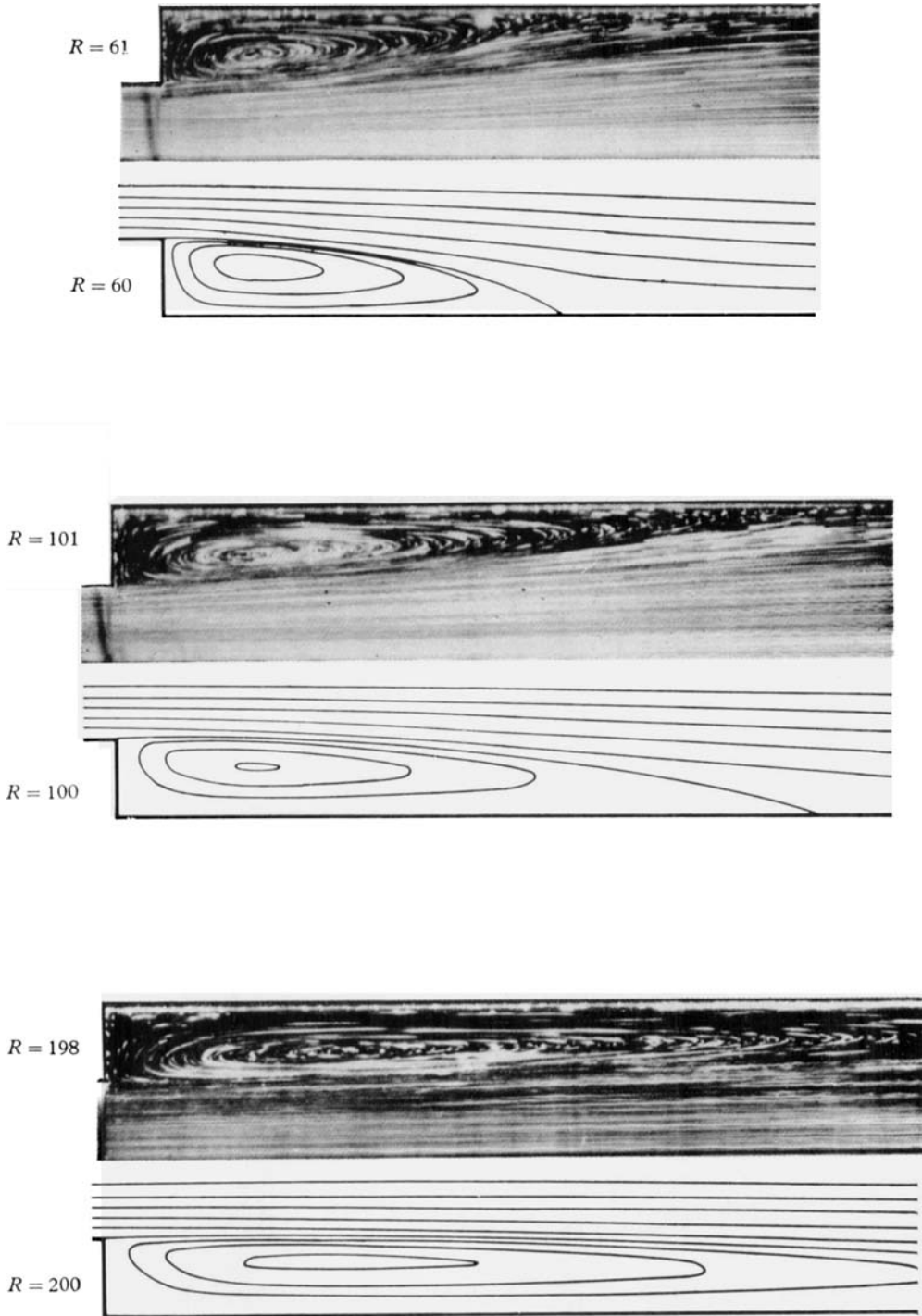
MACAGNO AND HUNG

FIGURE 9. Comparison of experimental and computational flow patterns.

MACAGNO AND HUNG